Journal of Colloid and Interface Science 513 (2018) 715–725

Contents lists available at ScienceDirect

Journal of Colloid and Interface Science

journal homepage: www.elsevier.com/locate/jcis

Regular Article

# Broadening the photoresponsive activity of anatase titanium dioxide particles via decoration with partial gold shells

Orawan Khantamat [a,b,1], Chien-Hung Li [a,1], Si-Ping Liu [c], Tingting Liu [a], Han Ju Lee [a], Oussama Zenasni [a], Tai-Chou Lee [c], Chengzhi Cai [a,*], T. Randall Lee [a,*]

[a] Department of Chemistry and the Texas Center for Superconductivity, University of Houston, Houston, TX 77204-5003, USA
[b] Department of Biochemistry, Faculty of Medicine, Chiang Mai University, Chiang Mai 50200, Thailand
[c] Department of Chemical and Materials Engineering, National Central University, Jhongli City 32001, Taiwan

## GRAPHICAL ABSTRACT

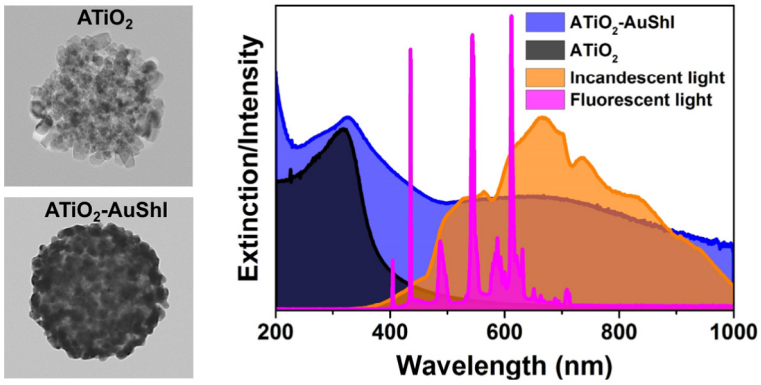


## ARTICLE INFO

*Article history:*
Received 22 June 2017
Revised 13 October 2017
Accepted 13 October 2017
Available online 27 October 2017

*Keywords:*
$TiO_2$
Partial gold shells
Visible light
Photocatalysis
Plasmon resonance

## ABSTRACT

Titanium dioxide ($TiO_2$) has gained increasing interest in materials research due to its outstanding properties and promising applications in a wide range of fields. From this perspective, we report the synthesis of custom-designed anatase $TiO_2$ submicrometer particles coated with partial Au shells ($ATiO_2$-AuShl). The synthetic strategy used herein yields uniformly shaped monodisperse particles. Amorphous $TiO_2$ core particles were synthesized using template-free oxidation and hydrolysis of titanium nitride (TiN); subsequent hydrothermal treatment generated anatase $TiO_2$ ($ATiO_2$) particles. Coating $ATiO_2$ particles with partial Au shells was accomplished using a simple seeded-growth method. Evaluation of the optical properties of these $ATiO_2$-AuShl particles showed that these submicrometer composites exhibited an intense absorption peak for $TiO_2$ in the UV region (~326 nm) and a broad extinction band in the visible range (~650 nm) arising from the incomplete Au shell. These $ATiO_2$-AuShl composite particles provide a unique and effective means for broadening the optical response of $TiO_2$-based nano- and micron-scale materials. The simplicity of our synthetic method should broaden the application of $ATiO_2$-AuShl particles in various visible light-driven technologies.



* Corresponding authors.
*E-mail addresses:* cai@uh.edu (C. Cai), trlee@uh.edu (T.R. Lee).
[1] These authors contributed equally to this work.

https://doi.org/10.1016/j.jcis.2017.10.053
0021-9797/

## 1. Introduction

$TiO_2$ is a promising material for many emerging applications. Since Fujishima and Honda discovered the photocatalytic splitting of water on a $TiO_2$ electrode in 1972 [1], the fundamental processes of $TiO_2$ photoelectrochemistry have been studied intensively. To date, $TiO_2$ has been exploited for photocatalytic water splitting, purification of pollutants, photocatalytic self-cleaning, and photocatalytic antibacterial applications as well as photovoltaics, photochromics, electrochromics, and various types of sensors [2–8]. Furthermore, $TiO_2$-based materials are now widely used due to their nontoxicity, chemical and biological stability, and low cost [9].

$TiO_2$ exists in three main polymorphs: rutile (tetragonal), anatase (tetragonal), and brookite (orthorombic). Rutile is the most stable form, whereas anatase and brookite are metastable and readily transformed to rutile when heated [10]. The phase normally found in the sol-gel syntheses of $TiO_2$ is anatase, which possesses a band gap of 3.2 eV, corresponding to an absorption wavelength of 385 nm. Rutile $TiO_2$ has a smaller band gap of 3.0 eV, with excitation wavelengths that extend into the visible (410 nm). As for brookite, theoretical and experimental studies have reported band gap values both smaller and larger than that of anatase. The band gap of brookite was first estimated by extended Hückel molecular orbital calculations as 3.14 eV [11], which falls between those of anatase and rutile. Nevertheless, anatase exhibits higher photocatalytic activity when compared to rutile or brookite [12,13], which might be attributed to its higher surface adsorptive capacity and higher rate of hole trapping. For example, Degussa P25, the most popular commercial $TiO_2$ material, with a 70% anatase and 30% rutile composition, possesses excellent photocatalytic activity [14,15] due to its mixed-phase composition and high anatase crystallinity. These properties favor photo-induced charge separation and a large specific surface area.

Most $TiO_2$ nano- and micron-scale structures have a high surface-to-volume ratio, providing a large surface area on which photo-induced reactions can occur. This feature enhances the rate of light absorption, increases photo-induced carrier density on the surface, increases the photo-reduction rate, and leads to higher surface photoactivity. In addition, the high surface-to-volume ratio of the particles enhances the surface absorption of hydroxide ($OH^-$) ions and $H_2O$ molecules, which also increases the photocatalytic reaction rate. The properties of $TiO_2$ particles are also influenced by the size, morphology, phase structure, surface chemical state, and synthesis process. For example, among the various $TiO_2$ particle morphologies investigated in recent years (e.g., tubes [16,17], rods [18,19], spheres [20,21], wires [22,23], and sheets [24,25]), spherical $TiO_2$ particles have been found to exhibit superior performance in environmental and energy applications due to their large specific surface area [26,27].

Monodisperse $TiO_2$ particles can be synthesized using a variety of methods, including sol-gel, hydrothermal, solvothermal, chemical vapor deposition, or template-based methods [28–31]. The traditional sol-gel route proceeds via hydrolysis of a titanium alkoxide precursor [9,28,32]. This process is typically fast but moisture-sensitive, making it difficult to control the size of the generated $TiO_2$ particles. Although the strategy of constructing amorphous $TiO_2$ particles and subsequent hydrothermal treatment provides a simple route for generating particles with targeted sizes, achieving monodispersity with this conventional method remains a challenge [26,33]. Other routes for preparing $TiO_2$ particles using templates, such as polystyrene (PS) [31] or $SiO_2$ [34] spheres, have been well documented, but are cost-prohibitive due to the high price of Ti-precursors. Moreover, the complicated synthetic conditions and use of an additional structural directing agent or surfactant often limit the use of this strategy in practical applications.

Although $TiO_2$ materials exhibit excellent properties as photoactivated catalytic materials, one major limitation involving the use of $TiO_2$ is the need for activation with UV light, since the absorption peak is narrow and lies largely in the near-UV region. To address this issue, researchers have attempted to increase the efficiency of $TiO_2$ by shifting its absorption window to the visible region through the incorporation of non-metal and transition metal dopants such as nitrogen, carbon, chromium, and iron [35–38]. These dopants decrease the band gap of $TiO_2$, which shifts the absorption toward the visible region of the spectrum, which can increase the efficiency of the photoactivity of the modified $TiO_2$. However, transition metal dopants can also act as electron-hole recombination sites for the photo-induced charge carriers and thus decrease the photocatalytic activity [39].

Alternatively, researchers have loaded $TiO_2$ with metal nanoparticles such as gold, silver, platinum, and palladium because such nanoparticles can act as electron sinks to enhance charge transfer and thus decrease the possibility of charge-hole recombination [40–43]. Furthermore, researchers recently have discovered the generation of photoexited electrons (hot electrons) from plasmonic nanomaterials such as gold and silver [44–46]. Energy transfer to hot electrons arises from the light-driven surface plasmon resonance excitation of the nanomaterials. Importantly, the injection of hot electrons to $TiO_2$ has been shown to inhibit electron-hole recombination to enhance the efficiency of photocatalytic activities [44–46].

In the studies reported herein, we optimized a simple alkoxide-free sol-gel synthetic method requiring no templates or structure-directing agents to prepare submicrometer $TiO_2$ particles with selected dimensions and properties. Using our synthetic route, the size of these amorphous $TiO_2$ particles can be easily tuned by adjusting the Ti species or reaction temperature. These amorphous $TiO_2$ particles readily undergo phase transformation via hydrothermal treatment. Inspired by the plasmonic properties of gold nanomaterials, the hydrothermally-treated $TiO_2$ particles ($ATiO_2$) were decorated with an incomplete Au shell on the $ATiO_2$ surface ($ATiO_2$-Au shells, $ATiO_2$-AuShl particles). To the best of our knowledge, this is the first report on the use of simple seeded-growth method for coating $ATiO_2$ particles with partial Au shells. Like $TiO_2$, gold is known to be non-toxic and environmentally friendly [47,48]. With Au shell decoration, these $TiO_2$-AuShl particles have the capacity to augment the optical properties of $TiO_2$ particles by broadening the range of absorbed UV–Vis (solar/white) light, thereby increasing their efficiency in photo-driven applications under a variety of conditions, such as the photocatalytic degradation of organic pollutants and the photocatalytic production of hydrogen. The overall strategy used to prepare our $ATiO_2$-AuShl particles is illustrated in Scheme 1.

## 2. Experimental

### 2.1. Materials

The following analytical-grade chemicals were purchased from the indicated suppliers and used without purification: titanium nitride, TiN (99%, Aldrich); hydrogen peroxide, $H_2O_2$ (30%, Macron Fine Chemicals); ammonium hydroxide, $NH_4OH$ (28–30%, BDH® VWR Analytical); (3-aminopropyl)trimethoxysilane, APTMS (97%, Aldrich); tetrakis(hydroxymethyl)phosphonium chloride, THPC (80%, Aldrich); hydrogen tetrachloroaurate(III) hydrate, $HAuCl_4 \cdot xH_2O$ (49% Au, Strem Chemicals); potassium carbonate, $K_2CO_3$ (≥99.0%, J.T. Baker); formaldehyde (35–40%, Macron Fine Chemicals); methylene blue, MB (ACROS Organics™); potassium sulfite, $K_2SO_3$ (Sigma Aldrich); sodium sulfide hydrate, $Na_2S \cdot xH_2O$ (Sigma Aldrich). Water was purified to a resistivity of 18 MΩ·cm

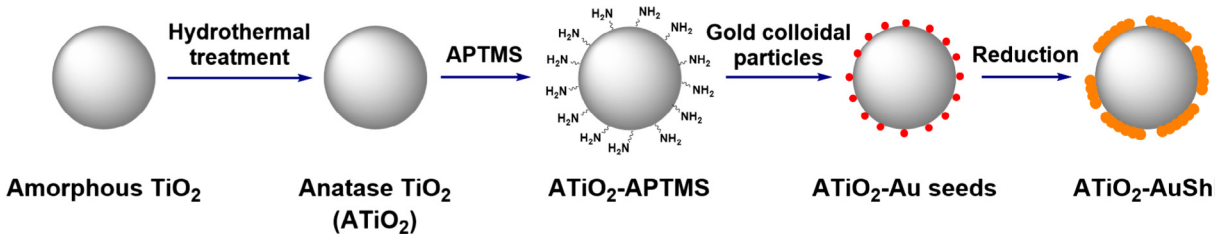


**Scheme 1.** Synthetic strategy used to prepare $ATiO_2$-Au shells ($ATiO_2$-AuShl particles).

(Millipore water; Academic Milli-Q Water System, Millipore Corporation). Prior to use, all glassware was cleaned using aqua regia solution (HCl:$HNO_3$; 3:1), thoroughly rinsed with Millipore water, and then dried.

### 2.2. Synthesis of anatase $TiO_2$ particles

#### 2.2.1. Preparation of Ti-peroxo solution

The synthetic procedure began with the preparation of the Ti-peroxo complex solution by dissolving commercial TiN in water in the presence of hydrogen peroxide ($H_2O_2$) and aqueous ammonia ($NH_4OH$). Specifically, the TiN (0.10 g) was dispersed in 100 mL of Millipore water followed by the addition of 10 mL of 30% hydrogen peroxide ($H_2O_2$) and 10 mL of 25% aqueous ammonia solution. After 2 h of vigorous stirring, the transparent yellow solutions of Ti-peroxo complex were obtained.

#### 2.2.2. Synthesis of amorphous submicrometer $TiO_2$ particles

Amorphous submicrometer $TiO_2$ particles were synthesized via hydrolysis of the Ti-peroxo complex. Briefly, an aliquot of Ti-peroxo complex solution was mixed with ethanol (1:2 volume ratio) under vigorous stirring at 80 °C. After heating for 20 h, the solution was cooled to room temperature and centrifuged to collect a white precipitate of amorphous $TiO_2$ particles. The precipitate was washed several times with ethanol. The as-synthesized amorphous $TiO_2$ particles were then dried overnight at 60 °C in a hot air oven.

#### 2.2.3. Hydrothermal treatment of $TiO_2$ particles for the transformation of crystallinity

To obtain photocatalytically-active submicrometer anatase $TiO_2$ particles, amorphous $TiO_2$ particles were subjected to further hydrothermal treatment. Typically, the as-synthesized amorphous $TiO_2$ particles were redispersed in Millipore water by magnetic stirring. The well-dispersed $TiO_2$ particles were then transferred to a Teflon-lined autoclave followed by heating at 200 °C for 24 h to transform the particles to anatase $TiO_2$ particles ($ATiO_2$). After cooling the Teflon-lined autoclave to room temperature, the precipitate was collected and washed several times with Millipore water and ethanol to isolate the particles. The resulting $ATiO_2$ particles were redispersed in ethanol.

### 2.3. Synthesis of submicrometer $ATiO_2$ particles coated with partial Au shells

#### 2.3.1. APTMS-functionalized $ATiO_2$ particles ($ATiO_2$-APTMS)

The $TiO_2$ particles surfaces were modified with APTMS to give amino-functionalized surfaces. An aliquot of APTMS (2 mL) was added to a vigorously stirred sample of $ATiO_2$ particles (~100–150 mg) in ethanol (100 mL). The mixture was allowed to react at room temperature under ambient conditions for 2 h, and then gently refluxed for 3 h to enhance the covalent bonding of the APTMS groups to the $TiO_2$ particle surface. The resulting $ATiO_2$-APTMS particles were isolated by centrifugation, washed several times with ethanol, and then redispersed in ethanol.

#### 2.3.2. Submicrometer $ATiO_2$ particles coated with gold-seeds ($ATiO_2$-Au seeds)

To synthesize submicrometer $ATiO_2$ particles coated with partial Au shells, we first deposited colloidal gold on the $ATiO_2$-APTMS particles using a self-assembly method [49]. A solution of colloidal gold particles (1–3 nm diameter) was prepared by the reduction of a 1 wt% aqueous solution of $HAuCl_4$ with THPC. Under rapid stirring, 1 mL of 1 M NaOH was added to 90 mL of Millipore water, followed by the addition of 2 mL of a 1.25% aqueous THPC solution. The mixture was stirred for 5 min, and then 4 mL of 1 wt% $HAuCl_4$ in water was added quickly to the stirred solution. The solution (~100 mL) containing the colloidal particles was stored at 4 °C for 2 days and then concentrated to 10 mL using a rotary evaporator.

A portion of the concentrated gold colloidal solution (5 mL) was then mixed with a 2-mL aliquot of $ATiO_2$-APTMS solution (5 mg/mL). After vigorous stirring for 1 h, the solution was allowed to equilibrate for 2–5 days to allow the gold colloidal particles to attach to the $TiO_2$ surface. The resulting $ATiO_2$-Au seeds particles were then washed by centrifugation and redispersed in Millipore water.

#### 2.3.3. Submicrometer $ATiO_2$ particles coated with partial Au shells ($ATiO_2$-AuShl)

To grow the gold overlayer on the $ATiO_2$-Au seeds particles, a solution containing a reducible gold salt (K-gold solution; 0.01% $K_2CO_3$, 0.05 mM $HAuCl_4$) was first prepared by dissolving 10 mg of anhydrous potassium carbonate in 100 mL of Millipore water. After 10 min of stirring, 167 μL of 1 wt% $HAuCl_4$ solution was added, and the solution was aged at 4 °C in the dark for 16 h. The growth of the gold shell layer on the gold-seeded particles proceeded via the reduction and deposition of $Au^{3+}$ by formaldehyde [50]. To a vigorously stirred 4-mL aliquot of the colorless K-gold solution, the seeded particle solution was added, followed by the addition of 10 μL of formaldehyde. Over the course of 1–5 min, the solution changed from colorless to slightly blue, which is characteristic of partial Au shell formation [49]. The resulting $ATiO_2$-AuShl particles were separated from the solvent by centrifugation and redispersion in Millipore water.

### 2.4. Photocatalytic degradation of methylene blue (MB) by $ATiO_2$-AuShl particles

To provide a preliminary assessment of the photocatalytic activity of $ATiO_2$-AuShl particles, we monitored the degradation of methylene blue upon exposure to visible light. Briefly, 12 mL of a solution of $TiO_2$ particles was prepared by mixing the particles with a 0.005 mg/mL an aqueous solution of MB. The particle concentration was adjusted to $5 \times 10^{10}$ particles/mL (~0.3 mg/mL), and the resulting mixture was sonicated for 10 min in the dark.

Subsequently, a 4-mL aliquot of the mixture was centrifuged, and the supernatant was used as a reference for UV–Vis spectroscopic analysis. The remaining mixture was then divided into two separate portions for incubation in the dark and under 60 W incandescent white light (or fluorescent light) for 4 h. The samples were then centrifuged, and the supernatant was collected for analysis by UV–Vis spectroscopy.

### 2.5. Photocatalytic hydrogen production by ATiO$_2$-AuShl particles

The preliminary assessment of the photocatalytic reaction for hydrogen production was conducted in a 225-mL custom-built cylindrical glass cell with a quartz side window and an illumination area of 23 cm$^2$. The sacrificial agent needed to drive the reaction was prepared by adding potassium sulfite (55 mmol) and sodium sulfide (77 mmol) to DI water (220 mL). An aliquot of 1 mL of ATiO$_2$-AuShl particles in aqueous solution ($1 \times 10^{10}$ particles/mL) was then added to the sacrificial solution, and the photocatalytic reactor was irradiated with a 300 W Xe lamp. The intensity was set at 100 mW/cm$^2$ and monitored by an optical meter (Newport 1918-R). The temperature was maintained at 25 °C during the reaction, and $H_2$ gas was collected for at least 5 h using a water displacement method. The evolved gas was analyzed using a China Chromatography GC 3000 gas chromatograph.

### 2.6. Characterization methods

The dimensions and morphologies of the as-prepared particles were characterized using scanning electron microscopy (SEM; LEO-1525) operating at an accelerating voltage of 15 kV, and transmission electron microscopy (TEM; JOEL-2000 FX) operating at an accelerating voltage of 200 kV. To obtain high-resolution images from the SEM analyses, all samples were deposited on a silicon wafer and allowed to dry. For the TEM analyses, the particles were deposited on 300 mesh holey carbon-coated copper grids and allowed to dry. To determine the size distribution and surface charge of the particles, dynamic light scattering (DLS) and zeta potential data were collected using a Zetasizer Nano ZS (Malvern Instruments) operating with a 514.5 nm light source at a fixed scattering angle of 90°. The concentration of the particles was measured using a NanoSight (Malvern Instruments).

The phase structure of the particles was analyzed using X-ray diffraction (XRD; D5000 X-ray diffractometer, Siemens (now Bruker), Karlsruhe, Germany). A concentrated sample of particles in ethanol was deposited on a Piranha-cleaned glass slide, and XRD was carried out using Cu Kα radiation (λ = 1.540562 Å) in the 2θ range from 10° to 100°. [*Caution: Piranha solution is highly corrosive, should never be stored, and should be handled with extreme care.*]

The composition of the interfaces of the synthesized particles was examined using X-ray photoelectron spectroscopy (XPS; PHI 5700 XPS) equipped with a monochromatic Al Kα X-ray source (hν = 1486.7 eV) incident at 90° relative to the axis of a hemispherical energy analyzer. For XPS analyses, a concentrated sample of particles in water was deposited on a copper-tape-covered silicon wafer and allowed to dry under ambient conditions. The number of scans used to collect the data for each element was: Au (1), C (1), N (4), O (1), Si (2), and Ti (2). The XPS data were processed by Multipak software, and the binding energy of all spectra were calibrated on Ti $2p_{3/2}$ at 458.8 eV [51]. Optical extinction spectra of suspensions containing the dispersed particles were collected using a Cary 50 Scan UV–visible (UV–Vis) spectrometer over the wavelength range of 200–1000 nm. Photoluminescence (PL) spectra were obtained at a concentration of $2 \times 10^9$ particles/mL using a PL spectrometer (PerkinElmer LS-55) with 353 nm incident light from a Xe flash lamp used for the excitation.

## 3. Results and discussion

### 3.1. Synthesis of amorphous submicrometer TiO$_2$ particles

Studies have shown that the properties of $TiO_2$ particles are governed by their size, morphology, and crystalline phase [52–54]. The conventional sol-gel method, the most widely applied approach for preparing amorphous $TiO_2$ particles, relies on the hydrolysis of a Ti precursor with subsequent condensation to form an inorganic framework. However, the $TiO_2$ particles prepared using this method tend to agglomerate and generally lack uniformity in size and shape [9]. In fact, there are several parameters that affect this sol-gel process. The concentration of the Ti precursor/species greatly impacts the crystallization behavior and the resulting characteristics of the synthesized particles [55]. The size, stability, and morphology of the produced sol from the Ti precursors are strongly affected by the water-to-Ti molar ratio ($r = [H_2O]/[Ti]$) [56,57]. Also, the peptization process (carried out by heating the solution or using a peptization agent) has a strong effect on the characteristics of the $TiO_2$ particles prepared via the sol-gel method [58]. In summary, obtaining $TiO_2$ particles with controlled size and narrow polydispersity is critical and can be accomplished by optimizing the synthesis conditions.

Using a modified protocol of the facile solution route developed by Wang et al. [26], we prepared monodisperse amorphous $TiO_2$ particles having targeted sizes. In this process, titanium nitride (TiN) is oxidized to $Ti^{4+}$ by dissolving the material in purified water in the presence of $H_2O_2$ and $NH_4OH$. These alkaline conditions transform the $Ti^{4+}$ rapidly to the transparent yellow color of a stable Ti precursor, Ti-peroxo complex $[Ti(OH)_3O_2]^-$, which is soluble in water but sparingly soluble in alcohol. Thus, the addition of ethanol to an aqueous solution of the Ti-peroxo complex turns the color of the solution from yellowish to milky. After heating, the hydrolysis and condensation reactions afford small, amorphous $TiO_2$ particles that gradually increase in size to form amorphous $TiO_2$ particles as a white precipitate. The formation of the particles can be described as follows:

$$Ti^{4+}_{aq} + H_2O_2 + 5\ OH^- \rightarrow [Ti(OH)_3O_2]^- + 2\ H_2O \quad (1)$$

$$2\ [Ti(OH)_3O_2]^- \rightarrow 2\ TiO_2 + 2\ H_2O + O_2 + 2\ OH^- \quad (2)$$

$$2\ Ti^{4+}_{aq} + 2\ H_2O_2 + 10\ OH^- \rightarrow 2\ TiO_2 + 6\ H_2O + O_2 + 2\ OH^- \quad (3)$$

The growth of the $TiO_2$ particles is controlled by the concentration of Ti species in solution. In our study, a high concentration of Ti precursor (0.2 wt% TiN) gave relatively large and inhomogeneous $TiO_2$ particles (Fig. S1) due to the simultaneous nucleation and growth that occurs with an abundance of monomer. In contrast, a low concentration of initial Ti species (0.075 wt% TiN) leads to heterogeneous nucleation, followed by growth, where the spontaneous growth process is dominant. These phenomena gave $TiO_2$ particles that are more homogeneous and smaller in size (Fig. S2a).

When keeping the concentration of the TiN constant at 0.075 wt %, an increase in the reaction temperature (from 80 to 90 °C) gave systematically smaller $TiO_2$ particles due to the rapid continuous nucleation of $TiO_2$, leading to a decrease in average size of the amorphous $TiO_2$ particles (Fig. S2a–c). In this synthetic methodology, the ratio of the solvent (such as ethanol or isopropanol) to Ti species is restricted to a relatively narrow range [26]. For our experiments, the ratio of Ti species to ethanol was set at 1:2. The influence of the concentration of initial Ti species and the reaction temperature on the average size of $TiO_2$ particles is summarized in Table S1, where the average particle diameter was determined from both SEM images and DLS measurements.

The ability to control different sizes and shapes of $TiO_2$ particles is pivotal to realizing their targeted applications. Therefore, $TiO_2$ particles of many different sizes and shapes have been synthesized to take advantage of their size- and shape-dependent properties [59]. For example, a fine level of size control in the range of 10–100 nm is considered necessary for synthetic nanobiology [60]. Furthermore, if the size of the particles decreases, which increases the specific surface area, then the increase in surface energy of such particles can facilitate their aggregation [61]. This phenomenon can cause agglomeration of small $TiO_2$ particles, which limits their applications. On the other hand, large $TiO_2$ particles, which are superior for photocatalysis due to the long charge-recombination times associated with the longer diffusion length of electrons in such $TiO_2$ particles [62], are also unstable in the liquid phase because they agglomerate due to their enhanced van der Waals attraction [63]. These considerations necessitate the synthesis of $TiO_2$ particles having specific sizes and optical properties. In this study, we sought to prepare amorphous $TiO_2$ particles in the range of 200–250 nm since these particles could be well dispersed in the aqueous phase. Fig. 1a shows a typical SEM image of the amorphous $TiO_2$ particles prepared in our hands using 0.1 wt% TiN at 80 °C with a 1:2 volume ratio of Ti-peroxo complex solution to ethanol. The as-synthesized amorphous $TiO_2$ particles exhibit a smooth outer surface with only few irregularities in the interfacial structure with an average size of 245 ± 46 nm and 276 ± 55 nm as measured by SEM (Fig. 1a) and DLS (Fig. 1b), respectively.

### 3.2. Morphology and crystallinity of submicrometer anatase $TiO_2$ particles

Several studies have highlighted the importance of crystallinity in tuning the photocatalytic properties of $TiO_2$ [52,53]. The hypothesis is that larger crystals provide the required charge separation and increase the time taken for $e^-h^+$ pairs to recombine, thereby giving rise to enhanced photocatalytic properties. Additionally, studies have shown that particles having high anatase content also have a low number of hydroxyl groups, and this latter feature is responsible for the superior properties. Less hydroxyl groups correspond to fewer photocatalysis-impairing peroxides. Therefore, in our efforts to synthesize $TiO_2$ particles with enhanced properties for photocatalytic applications, we directly tuned the crystallinity of the as-synthesized amorphous $TiO_2$ particles to anatase $TiO_2$ particles ($ATiO_2$) via hydrothermal treatment.

The hydrothermal treatment of amorphous $TiO_2$ particles introduced morphological changes to the outer surfaces of the $TiO_2$ particles with a change in particle size but not shape, which was retained. Fig. 2a and b show the morphologies of the $ATiO_2$ particles measured using SEM and TEM, respectively. After the hydrothermal reaction, the resultant $ATiO_2$ particles exhibit rough surfaces, which consist of a number of small protrusions. The average diameter of the $ATiO_2$ particles also diminished upon hydrothermal treatment from 245 ± 46 nm to 193 ± 43 nm, as measured by SEM. The diffraction patterns of the $ATiO_2$ structures obtained by XRD (see Fig. 2c) can be indexed to the anatase crystalline phase of $TiO_2$ (reference ICSD 9852) [64]. In addition, the observed sharp diffraction peaks indicate a high degree of crystallinity for the anatase $TiO_2$ particles. From the full width at half maximum (FWHM) of the strongest (1 0 1) diffraction of anatase, our $ATiO_2$ particle crystallite size was calculated using the Scherrer equation [65] to be ~20 nm.

Given that the $ATiO_2$ particles were derived directly from the homogeneous $TiO_2$ particles shown in Fig. 1, and that they failed to undergo degradation throughout the APTMS functionalization process and the subsequent Au shell growth process described below, argue strongly against their existence as aggregates. Furthermore, measurements of the size distribution of the $ATiO_2$ particles by DLS found no aggregates present in the solution (please see the DLS size distribution by intensity plot for the $ATiO_2$ particles in Fig. S3b, which shows a single peak).

### 3.3. Synthesis of submicrometer $TiO_2$ particles coated with partial Au shells

Gold nanoparticles (AuNPs) enjoy strong extinction maxima in the visible region due to a localized surface plasmon resonance (LSPR) that is generated by the collective oscillation of surface electrons. The exploitation of the LSPR of AuNPs to induce visible light photocatalytic activity in $TiO_2$ remains a challenging task because the LSPR is influenced by the size of the nanostructures. In this case, altering the size of the gold surface in contact with the $TiO_2$ particles might aid in optimizing the efficiency of the photoexcited ("hot") electron transfer from Au to $TiO_2$ [66–68]. Furthermore, using larger gold nanoparticles to decorate $TiO_2$ particles gives rise to enhanced photocatalytic activity due to the concomitantly stronger plasmonic near-fields [66,67]. Here, we designed and synthesized the structures to have $TiO_2$ cores sufficiently large to serve as templates for growing discontinuous Au shells (Au patches). The $TiO_2$ particles coated with partial Au shell structures might provide advantages over decorating the surfaces with small gold nanoparticles, given the broadened extinction spectrum (i.e., into the near infrared) of particles having the $TiO_2$-Au shell structure (i.e., $TiO_2$-AuShl).

Fabrication of the partial Au shells on the $TiO_2$ particles was accomplished using an established seeded-growth method [49]. In this synthetic strategy, APTMS-functionalized $TiO_2$ particles were initially prepared and then decorated with colloidal Au particles, prepared as described previously [49]. These attached gold nanoseeds were then used to nucleate the growth of a partial gold shell in the presence of $HAuCl_4$ and formaldehyde as the reducing agent.

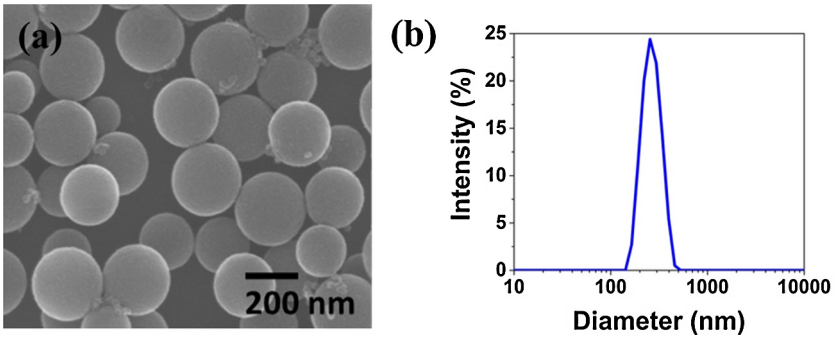


**Fig. 1.** Amorphous submicrometer $TiO_2$ particles: (a) SEM image and (b) DLS size distribution by intensity.

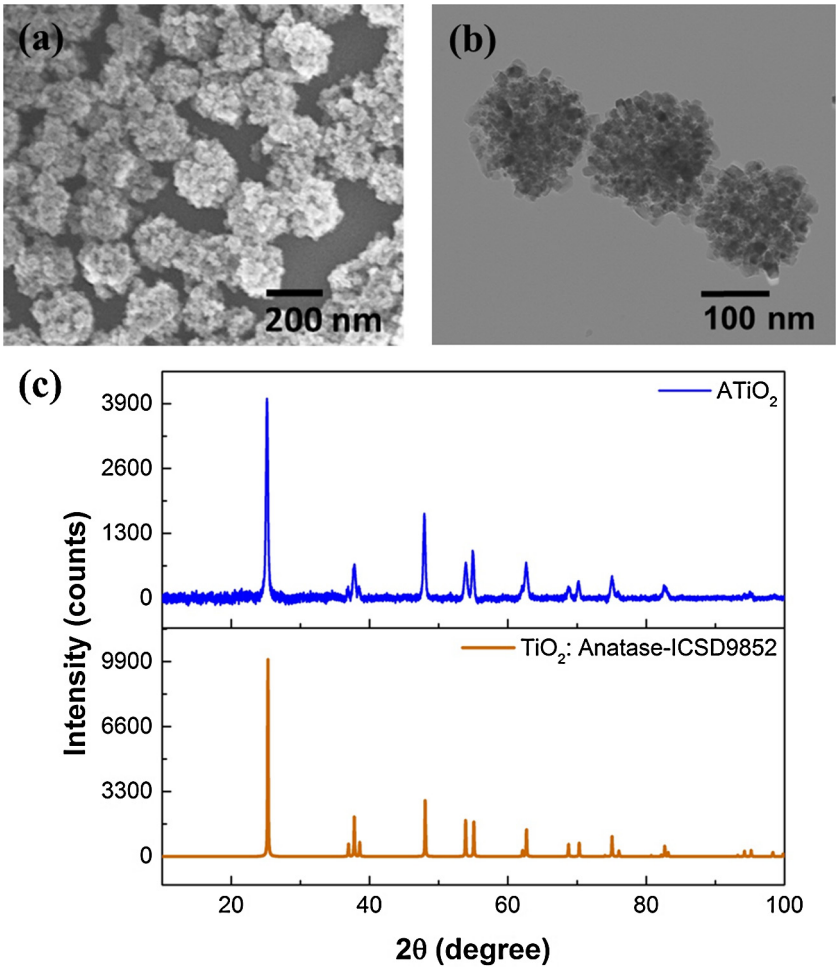


**Fig. 2.** $ATiO_2$ particles: (a) SEM image, (b) TEM image, and (c) XRD spectrum.

*3.3.1. Surface composition and charge of APTMS-Functionalized $ATiO_2$ particles*

To characterize the surface composition and charge of the APTMS-functionalized $ATiO_2$ particles, we collected data from analysis by XPS and zeta potential measurements, respectively. The high resolution XPS data of the synthesized $ATiO_2$-APTMS particles are shown in Fig. 3, and the corresponding survey spectrum is shown in Fig. S4. The XPS spectrum in the Ti 2p region for the $ATiO_2$ particles showed Ti $2p_{3/2}$ and Ti $2p_{1/2}$ spin-orbit splitting photoelectrons located at binding energies (BE) of 458.8 and 464.5 eV, respectively, with an energy difference of 5.7 eV [51]. The O 1s signal for $ATiO_2$-APTMS shows a peak at 530.1 eV and a shoulder located at a higher binding energy of 532.3 eV. The O 1s peak at 530.1 eV can be assigned to oxide species ($TiO_2$), and the peak at 532.3 eV is consistent with the reported O 1s binding energy for Si-O-Ti species [69], which reflects the bonding of APTMS to the surface of the $ATiO_2$ particles. The XPS spectrum in the N 1s region confirmed the presence of a nitrogen peak associated with the APTMS molecules attached to the surface of $ATiO_2$. The peak consisted of two types of nitrogen, where the lower binding energy at 399.9 eV is consistent with R-$NH_2$, and the higher binding energy at 401.6 eV is consistent with the positively charged nitrogen of $NH_3^+$ [70].

The average zeta potential (surface charge) of the $ATiO_2$-APTMS particles in aqueous solution was 43.5 ± 6.1 mV. These results indicate that the surfaces of particles are positively charged, plausibly due to the amino groups of APTMS. The large value for the zeta potential (≥30 mV) is consistent with a model in which the presence of charges on the surface confers colloidal stability to the APTMS-functionalized $TiO_2$ particles, preventing their aggregation [71,72]. TEM images of the subsequently prepared $ATiO_2$-Au seed particles are shown in Fig. S5, which reveals the presence of the colloidal Au seeds.

*3.3.2. Morphology, phase structure, surface composition, and surface charge of $ATiO_2$-AuShl*

Fig. 4a and b show SEM and TEM images, respectively, of the synthesized $ATiO_2$-AuShl particles. The SEM images depict a partial Au shell (i.e., Au patches) on the $TiO_2$ particles, with average diameters of 199 ± 26 nm (see also Fig. S6 in the Supporting Information). The gold coating is discontinuous with topographical roughness on the nanometer scale. The growth of the partial gold shell on the $TiO_2$ surface can be controlled by adjusting the ratio of the Au-seeded $TiO_2$ and K-Au solutions. At a low concentration of gold salt (0.05 mM $HAuCl_4$) and an excessive amount of reducing agent (29 mM formaldehyde), the incomplete shell structure surrounding the $TiO_2$ particles formed gradually. Notably, our interpretation of partial coverage is supported by XPS analysis, which is a surface-sensitive analytical technique (*vide infra*).

We used XRD to characterize the phase structure of the $ATiO_2$-AuShl particles (Fig. 4c). Due to the amount of Au deposition on the surface of $TiO_2$ particles, gold was the main diffraction pattern found in the $ATiO_2$-AuShl particles. Based on the XRD patterns, anatase peaks from our samples were still observed, especially

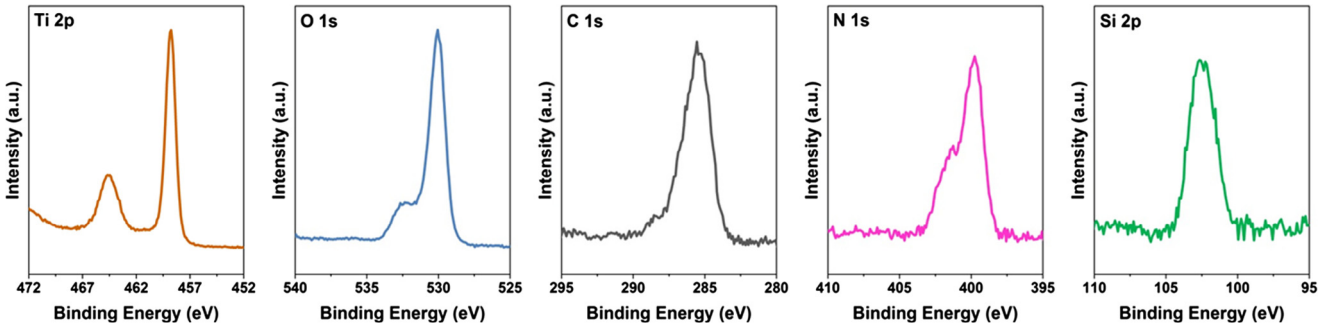


**Fig. 3.** XPS spectra of $ATiO_2$-APTMS particles for the spectral regions corresponding to the Ti 2p, O 1s, C 1s, N 1s, and Si 2p binding energies.

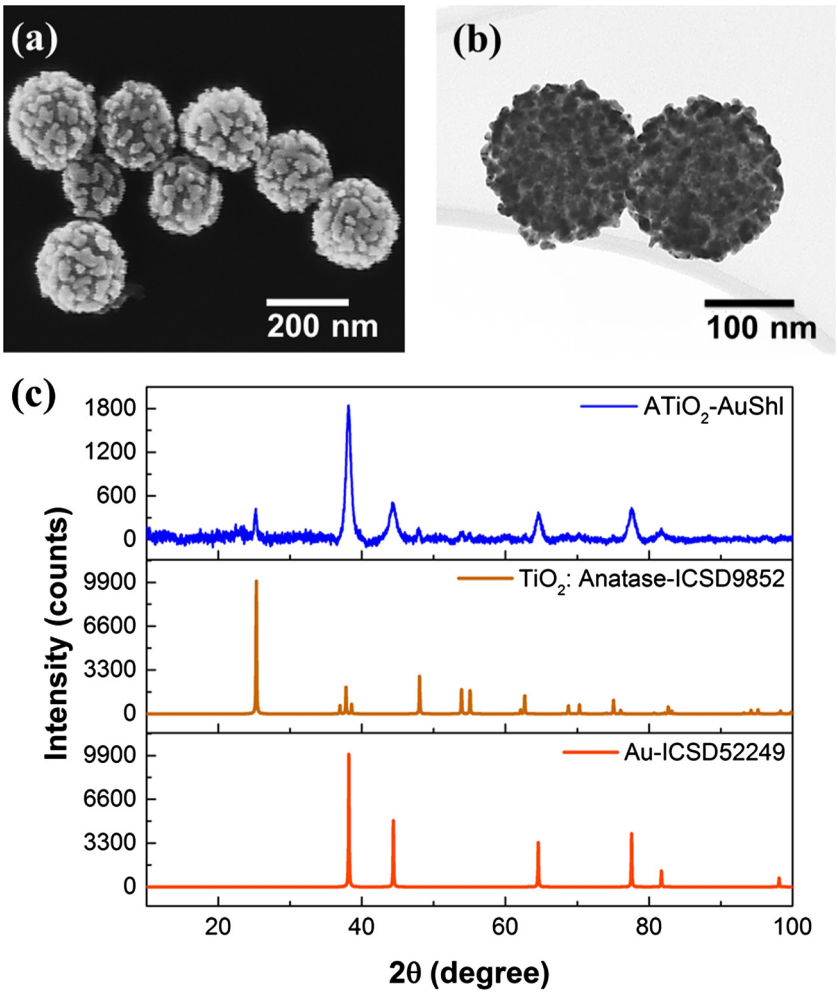


**Fig. 4.** $ATiO_2$-AuShl particles: (a) SEM image, (b) TEM image, and (c) XRD patterns of the $ATiO_2$-AuShl particles compared to anatase $TiO_2$ (ICSD 9852) and gold (ICSD 52249).

the peak at 25.3°. While the deposition of the partial Au shell gave weaker intensities for the anatase peaks (compared to Fig. 2c), the partial Au shell exerted no influence on the crystalline structure of $ATiO_2$.

The surface composition of these $ATiO_2$-AuShl particles was analyzed by XPS; Fig. 5 provides a high-resolution XPS spectrum of the Au 4f binding energy region, and Fig. S7 shows the corresponding survey spectrum. These results confirm the presence of gold on the $ATiO_2$ particles. Moreover, weak peaks are evident in the N 1s and Si 2p spectral regions – an observation that is consistent with the formation of an incomplete Au shell on the surfaces of the APTMS-functionalized $ATiO_2$ particles. The Ti-to-Au ratio calculated from the Ti 2p and Au 4f peak intensities was 0.25 for the $ATiO_2$-AuShl particles. From these data, we can estimate crudely that the Au shells cover more than 50% of the surface of the $ATiO_2$ particles (please see the Supporting Information for details).

The surface charge of the particles in aqueous solution was measured using a Zetasizer Nano ZS. The average surface charge of the APTMS-functionalized $ATiO_2$ particles was 43.5 ± 6.1 mV, indicating that the particles were positively charged. However, the surface of the $TiO_2$ particles became negatively charged after decorating with either colloidal gold (−21.2 ± 6.8) or a partial gold shell (−26.8 ± 7.1). The negative charges on the surface of the particles can be attributed to the presence of THPC-stabilized colloidal

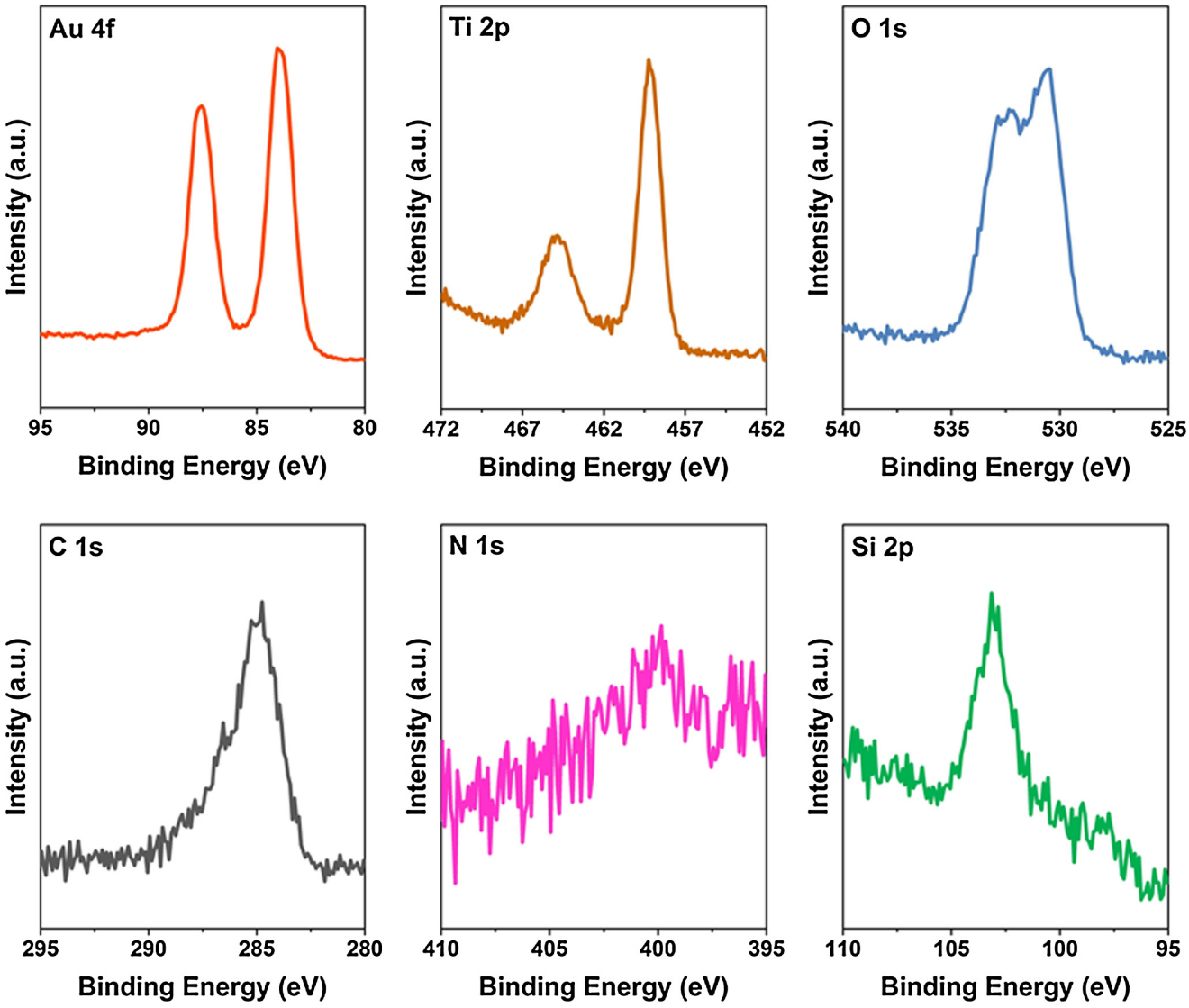


**Fig. 5.** XPS spectra for $ATiO_2$-AuShl particles over spectral regions corresponding to Au 4f, Ti 2p, O 1s, C 1s, N 1s, and Si 2p binding energies.

gold [73] or formate ligands present during the growth of the shell [49,74], respectively.

### 3.4. Optical properties of $ATiO_2$-AuShl particles

The optical properties of the $ATiO_2$-AuShl particles presented in Figs. 4 and S6 were examined by UV–Vis spectroscopy. Fig. 6 shows that the unmodified $ATiO_2$ particles exhibited a sharp absorption maximum at ~320 nm, which tapered off rapidly without extending into the visible region. As a consequence of the deposition of Au patches on the $TiO_2$ surface, the $ATiO_2$-AuShl particles exhibited not only a distinct peak at ~326 nm arising from $TiO_2$ [66,67], but also a broad peak centered at ~650 nm arising from the partial Au shell [75]. These results illustrate the effect of the LSPR of the Au shells on the extinction spectra of the $TiO_2$-AuShl structures [75]. $ATiO_2$-AuShl particles exhibited broad extinction spectra that extended to the visible region, affording good overlap with the emission wavelengths of incandescent and fluorescent light bulbs, which we used as a visible light source in applications involving photocatalysis (*vide infra*).

The effect of Au clusters on the extinction spectra of $TiO_2$-Au structures has been reported [66,67], but relatively few studies

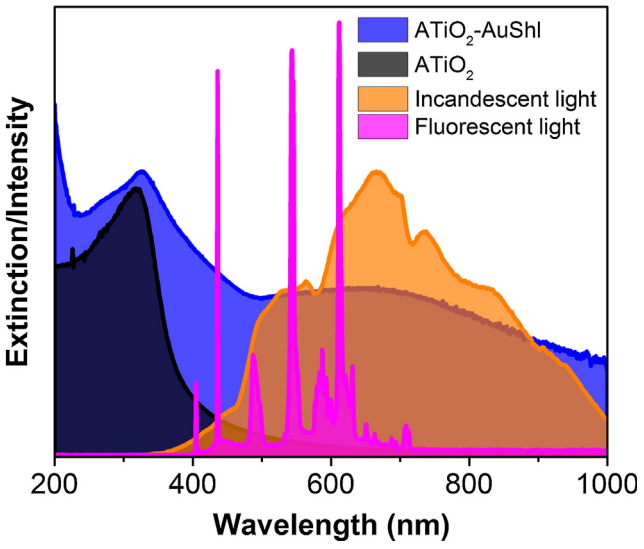


**Fig. 6.** Extinction spectra of $ATiO_2$ and $ATiO_2$-AuShl particles with the spectral overlap of light from an incandescent and fluorescent lamp.

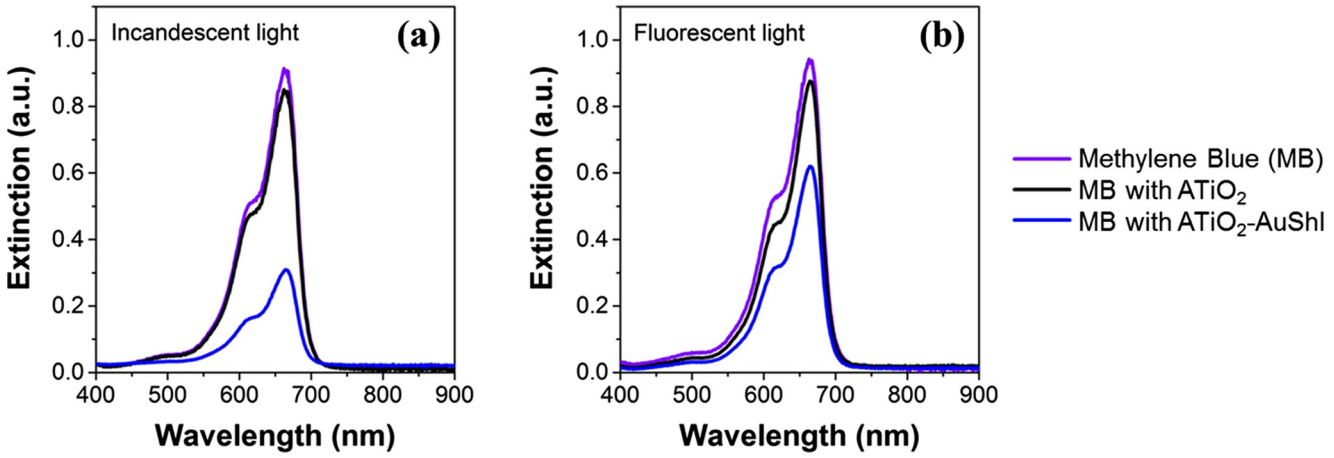


**Fig. 7.** Spectra of MB solutions after irradiation for 4 h with (a) incandescent light, and (b) fluorescent light in the presence of MB alone, $ATiO_2$ particles, and $ATiO_2$-AuShl particles.

have focused on spherical $TiO_2$ structures. Seh et al. [67] compared the LSPR of core-shell Au-$TiO_2$ structures with that of Janus particles in which $TiO_2$ was coated on only one side of the AuNPs. These researchers found a larger red-shift in the LSPR peak for core-shell structures when compared to their Janus counterparts. Claverie and co-workers [66] showed that the plasmonic extinction of Au-$TiO_2$ nanohybrids is enhanced by the presence of a whispering gallery mode (WGM) resonance by increasing the size of the $TiO_2$ and/or AuNP component(s). Furthermore, the observed enhancement in the latter nanohybrids strongly depends on the penetration of the AuNPs within the $TiO_2$ matrix. In our case, the roughness and incomplete Au shell together with its LSPR likely influences the extinction spectra of the $ATiO_2$-AuShl particles [75,76], giving rise to the broadening of the peak in the visible region. We note also that, upon growing the partial Au shell, we observed a small red shift in the absorption maximum of $TiO_2$, and the slope of the edge of the absorption related to the band gap of $TiO_2$ was flattened; the latter, however, might arise from interband transitions of Au [77].

### 3.5. Photocatalytic degradation of methylene blue by $ATiO_2$-AuShl particles

The photocatalytic activity of the $ATiO_2$-AuShl particles shown in Figs. 4 and S6 under visible light was characterized by measuring the degradation of MB in an aqueous suspension under incandescent and fluorescent light. Fig. 7 shows the effects of visible light in conjunction with the $ATiO_2$ particles and $ATiO_2$-AuShl particles on the absorption spectra of an aqueous solution of MB. The intensity of the absorption maxima of MB decreased markedly in response to illumination of both incandescent and fluorescent light in the presence of particularly the $ATiO_2$-AuShl particles, which can be interpreted as the degradation of MB. In contrast, there was no significant change in the extinction spectra of MB when illuminated by visible light in the presence of the simple $ATiO_2$ particles, and there was no spectral shifts or changes in intensity for MB in the presence of any of the particles under dark conditions (i.e., no illumination whatsoever). More importantly, the MB degradation in the presence of the $ATiO_2$-AuShl particles during incandescent light activation was observed to be greater than that of fluorescent light illumination due to the broad emission spectrum of incandescent light, which overlapped well with the extinction spectra of the $ATiO_2$-AuShl particles (Fig. 6).

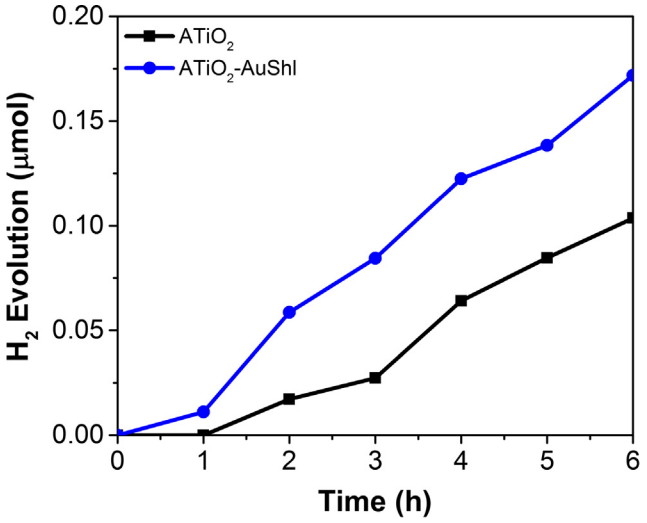


**Fig. 8.** $H_2$ evolution as a function of reaction time for $ATiO_2$ particles and $ATiO_2$-AuShl particles.

### 3.6. Photocatalytic hydrogen production by $ATiO_2$-AuShl particles

Data collected from a preliminary assessment the photocatalytic reaction for hydrogen production catalyzed by the $ATiO_2$-AuShl particles are shown in Fig. 8. The experiments were performed under irradiation using a 300-watt xenon lamp, with the resulting gas collected using a water-displacement method. The amounts of hydrogen gas collected for both $ATiO_2$ and $ATiO_2$-AuShl particles are shown in Fig. 8. The hydrogen evolution rate for reactions involving $ATiO_2$ and $ATiO_2$-AuShl particles remained steady for a period of 6 h. Importantly, the results indicate that the photocatalytic activity of the $ATiO_2$-AuShl particles is much greater than that of the $ATiO_2$ particles, especially after 1 h of reaction time.

### 3.7. Photoluminescence emission spectra and electron-hole recombination of $ATiO_2$-AuShl particles

Photoluminescence (PL) emission spectra have been widely used to investigate the efficiency of charge-carrier trapping, migration, and transfer, as well as to understand the fate of electron-hole pairs in semiconductor particles [78]. Anatase $TiO_2$ powder shows

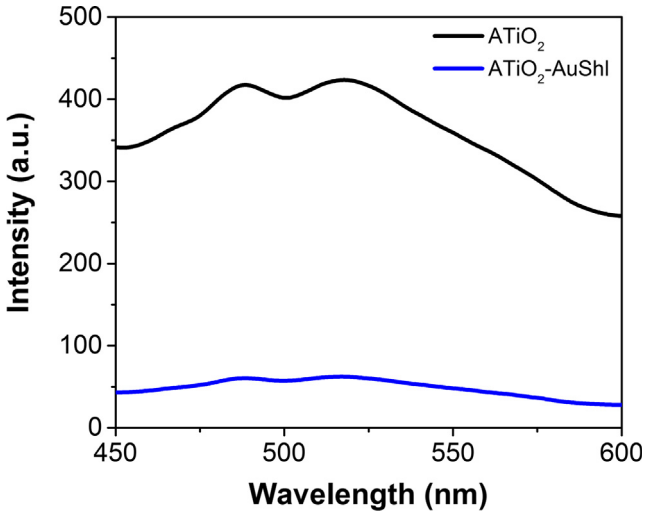


**Fig. 9.** PL spectra of aqueous solutions containing $ATiO_2$ and $ATiO_2$-AuShl particles.

a broad PL emission peak at ~500 nm [79]. In this study, we measured the PL emission spectra of $ATiO_2$ particles and $ATiO_2$-AuShl particles at room temperature using an excitation wavelength of 353 nm; Fig. 9 shows the PL emission spectra of $ATiO_2$ particles and $ATiO_2$-AuShl particles over the wavelength range of 450–600 nm. At the same concentration, the intensity of the PL spectra of the $ATiO_2$ particles was higher than that of the $ATiO_2$-AuShl particles (i.e., the PL intensities decreased due to the growth of the partial gold shells). In these systems, the PL emission arises from the radiative recombination of self-trapped excitons [80,81]. Therefore, the observed reduction in PL intensity indicates a decrease in the radiative recombination process. The results appear to be consistent with a model in which the Au shells create photoexcited electrons via plasmonic modulation [44–46] and capture photoexcited electrons from $TiO_2$ [82], giving rise to a recombination route that involves no PL. As a consequence, the probability for excited electrons to recombine radiatively with holes in $TiO_2$ is strongly suppressed. The PL emission spectra for $ATiO_2$-AuShl particles imply reduced recombination and increased photocatalytic activity, which is consistent with the enhanced photocatalytic activity observed above for the $ATiO_2$-AuShl structures in the degradation of MB and hydrogen evolution described above.

## 4. Conclusions

Submicrometer anatase $TiO_2$ particles coated with partial Au shells ($ATiO_2$-AuShl) were synthesized using a seeded-growth method without the need of any structure-directing templates or surfactants. The synthetic strategy used to prepare the composite particles gave structures with good uniformity and controlled dimensions of $TiO_2$ core particles, which provided a facile pathway to the targeted monodisperse $ATiO_2$-AuShl particles. Measurements of the optical properties of the $ATiO_2$-AuShl particles found intense absorptions in the UV region (~326 nm) associated with $TiO_2$ and broad extinctions in the visible range (~650 nm) associated with the deposition of Au. In studies of potential applications, the $ATiO_2$-AuShl particles were found to enhance both the photocatalytic degradation of methylene blue (a model organic pollutant) and the photocatalytic generation of hydrogen via water splitting. Importantly, the growth of the partial Au shells on the surface of the TiO2 core particles led to an overall broadening of the absorption of light across a range of wavelengths, giving access to mechanisms that inhibit electron-hole recombination and consequently enhance photocatalytic activity. The simplicity of the synthetic method, absence of toxic components, and tunability of particle size afforded by the strategies and materials reported here should permit the use $ATiO_2$-AuShl particles in various light-driven technologies in fields ranging from medicine to energy.

## Acknowledgments

The authors thank the Asian Office of Aerospace Research and Development (AFOSR/AOARD FA2386-16-1-4067), the Robert A. Welch Foundation (E-1320), the National Science Foundation (DMR-1508722), and the Texas Center for Superconductivity for generously supporting this research. Additionally, the Malvern Nanosight instrument used in this study was acquired using a Defense University Research Instrumentation Program (DURIP) grant (FA9550-15-1-0374) issued by the Air Force Office of Scientific Research.

## Appendix A. Supplementary material

Supplementary data associated with this article can be found, in the online version, at https://doi.org/10.1016/j.jcis.2017.10.053.

## References

[1] A. Fujishima, K. Honda, Electrochemical photolysis of water at a semiconductor electrode, Nature 238 (1972) 37–38.
[2] A. Fujishima, T.N. Rao, D.A. Tryk, $TiO_2$ photocatalysts and diamond electrodes, Electrochim. Acta 45 (2000) 4683–4690.
[3] A. Fujishima, T.N. Rao, D.A. Tryk, Recent progress in electrochemistry and photoelectrochemistry on polycrystalline boron-doped diamond surfaces, Electrochem. Soc. 99 (2000) 383–388.
[4] M. Grätzel, Photoelectrochemical cells, Nature 414 (2001) 338–344.
[5] D.A. Tryk, A. Fujishima, K. Honda, Recent topics in photoelectrochemistry: achievements and future prospects, Electrochim. Acta 45 (2000) 2363–2376.
[6] O. Carp, C.L. Huisman, A. Reller, Photoinduced reactivity of titanium dioxide, Prog. Solid State Chem. 32 (2004) 33–177.
[7] M. Grätzel, Solar energy conversion by dye-sensitized photovoltaic cells, Inorg. Chem. 44 (2005) 6841–6851.
[8] K. Hashimoto, H. Irie, A. Fujishima, $TiO_2$ photocatalysis: a historical overview and future prospects, Jpn. J. Appl. Phys. 44 (2005) 8269–8285.
[9] M. Cargnello, T.R. Gordon, C.B. Murray, Solution-phase synthesis of titanium dioxide nanoparticles and nanocrystals, Chem. Rev. 114 (2014) 9319–9345.
[10] D.A.H. Hanaor, C.C. Sorrell, Review of the anatase to rutile phase transformation, J. Mater. Sci. 46 (2011) 855–874.
[11] M. Grätzel, F.P. Rotzinger, The influence of the crystal-lattice structure on the conduction-band energy of oxides of titanium(IV), Chem. Phys. Lett. 118 (1985) 474–477.
[12] W. Li, C. Liu, Y. Zhou, Y. Bai, X. Feng, Z. Yang, L. Lu, X. Lu, K.Y. Chan, Enhanced photocatalytic activity in anatase/$TiO_2$(B) core-shell nanofiber, J. Phys. Chem. C 112 (2008) 20539–20545.
[13] S. Liu, J. Yu, M. Jaroniec, Anatase $TiO_2$ with dominant high-energy 001 facets: synthesis, properties, and applications, Chem. Mater. 23 (2011) 4085–4093.
[14] M.I. Litter, Heterogeneous photocatalysis: transition metal ions in photocatalytic systems, Appl. Catal. B 23 (1999) 89–114.
[15] J. Yu, H. Yu, B. Cheng, M. Zhou, X. Zhao, Enhanced photocatalytic activity of $TiO_2$ powder (P25) by hydrothermal treatment, J. Mol. Catal. A: Chem. 253 (2006) 112–118.
[16] N. Mir, K. Lee, I. Paramasivam, P. Schmuki, Optimizing $TiO_2$ nanotube top geometry for use in dye-sensitized solar cells, Chem. Eur. J. 18 (2012) 11862–11866.
[17] G.K. Mor, K. Shankar, M. Paulose, O.K. Varghese, C.A. Grimes, Enhanced photocleavage of water using titania nanotube arrays, Nano Lett. 5 (2005) 191–195.
[18] J. Jiu, S. Isoda, F. Wang, M. Adachi, Dye-sensitized solar cells based on a single-crystalline $TiO_2$ nanorod film, J. Phys. Chem. B 110 (2006) 2087–2092.
[19] Y. Li, X. Fang, N. Koshizaki, T. Sasaki, L. Li, S. Gao, Y. Shimizu, Y. Bando, D. Golberg, Periodic $TiO_2$ nanorod arrays with hexagonal nonclose-packed arrangements: excellent field emitters by parameter optimization, Adv. Funct. Mater. 19 (2009) 2467–2473.
[20] D. Chen, L. Cao, F. Huang, P. Imperia, Y.B. Cheng, R.A. Caruso, Synthesis of monodisperse mesoporous titania beads with controllable diameter, high surface areas, and variable pore diameters (14–23 nm), J. Am. Chem. Soc. 132 (2010) 4438–4444.
[21] X. Jiang, T. Herricks, Y. Xia, Monodispersed spherical colloids of titania: synthesis, characterization, and crystallization, Adv. Mater. 15 (2003) 1205–1209.
[22] H. Li, W. Lu, J. Tian, Y. Luo, A.M. Asiri, A.O. Al-Youbi, X. Sun, Synthesis and study of plasmon-induced carrier behavior at Ag/$TiO_2$ nanowires, Chem. Eur. J. 18 (2012) 8508–8514.

[23] H.B. Wu, H.H. Hng, X.W. Lou, Direct synthesis of anatase $TiO_2$ nanowires with enhanced photocatalytic activity, Adv. Mater. 24 (2012) 2567–2571.
[24] L. Etgar, W. Zhang, S. Gabriel, S.G. Hickey, M.K. Nazeeruddin, A. Eychmüller, B. Liu, M. Grätzel, High efficiency quantum dot heterojunction solar cell using anatase (001) $TiO_2$ nanosheets, Adv. Mater. 24 (2012) 2202–2206.
[25] X. Han, Q. Kuang, M. Jin, Z. Xie, L. Zheng, Synthesis of titania nanosheets with a high percentage of exposed (001) facets and related photocatalytic properties, J. Am. Chem. Soc. 131 (2009) 3152–3153.
[26] S. Wang, Y. Ding, S. Xu, Y. Zhang, G. Li, L. Hu, S. Dai, $TiO_2$ nanospheres: a facile size-tunable synthesis and effective light-harvesting layer for dye-sensitized solar cells, Chem. Eur. J. 20 (2014) 4916–4920.
[27] H. Zhu, Y. Shang, Y. Jing, Y. Liu, Y. Liu, A.M. El-Toni, F. Zhang, D. Zhao, Synthesis of monodisperse mesoporous $TiO_2$ nanospheres from a simple double-surfactant assembly-directed method for lithium storage, ACS Appl. Mater. Interfaces 8 (2016) 25586–25594.
[28] X. Chen, S.S. Mao, Synthesis of titanium dioxide ($TiO_2$) nanomaterials, J. Nanosci. Nanotechnol. 6 (2006) 906–925.
[29] M. Grätzel, Sol-gel processed $TiO_2$ films for photovoltaic applications, Sol-Gel Sci. Technol. 22 (2001) 7–13.
[30] X. Wu, G.Q. Lu, L. Wang, Shell-in-shell $TiO_2$ hollow spheres synthesized by one-pot hydrothermal method for dye-sensitized solar cell application, Energy Environ. Sci. 4 (2011) 3565–3572.
[31] Z. Zhong, Y. Yin, B. Gates, Y. Xia, Preparation of mesoscale hollow spheres of $TiO_2$ and $SnO_2$ by templating against crystalline arrays of polystyrene beads, Adv. Mater. 12 (2000) 206–209.
[32] X. Chen, S.S. Mao, Titanium dioxide nanomaterials: synthesis, properties, modifications, and applications, Chem. Rev. 107 (2007) 2891–2959.
[33] X.L. Li, Q. Peng, J.X. Yi, X. Wang, Y. Li, Near monodisperse $TiO_2$ nanoparticles and nanorods, Chem. Eur. J. 12 (2006) 2383–2391.
[34] D.P. Wang, H.C. Zeng, Multifunctional roles of $TiO_2$ nanoparticles for architecture of complex core-shells and hollow spheres of $SiO_2$-$TiO_2$-polyaniline system, Chem. Mater. 21 (2009) 4811–4823.
[35] R. Asahi, T. Morikawa, T. Ohwaki, K. Aoki, Y. Taga, Visible-light photocataysis in nitrogen-doped titanium oxides, Science 293 (2001) 269–271.
[36] S. Sakthivel, H. Kisch, Daylight photocatalysis by carbon-modified titanium dioxide, Angew. Chem. Int. Ed. 42 (2003) 4908–4911.
[37] Y.H. Peng, G.F. Huang, W.Q. Huang, Visible-light absorption and photocatalytic activity of Cr-doped $TiO_2$ nanocrystal films, Adv. Powder Technol. 23 (2012) 8–12.
[38] W. Zhang, Y. Chen, S. Yu, S. Chen, Y. Yin, Preparation and antibacterial behavior of $Fe^{3+}$-doped nanostructured $TiO_2$ thin films, Thin Solid Films 516 (2008) 4690–4694.
[39] M. Pelaez, N.T. Nolan, S.C. Pillai, M.K. Seery, P. Falaras, A.G. Kontos, P.S.M. Dunlop, J.W.J. Hamilton, J.A. Byrne, K. O'shea, M.H. Entezari, D.D. Dinoysiou, A review on the visible light active titanium dioxide photocatalysts for environmental applications, Appl. Catal., B 125 (2012) 331–349.
[40] V. Subramanian, E.E. Wolf, P.V. Kamat, Catalysis with $TiO_2$/gold nanocomposites. effect of metal particle size on the Fermi level equilibration, J. Am. Chem. Soc. 126 (2004) 4943–4950.
[41] X. You, F. Chen, J. Zhang, M. Anpo, A novel deposition preciptitation method for preparation of Ag-loaded titanium dioxide, Catal. Lett. 102 (2005) 247–250.
[42] Y. Zeng, W. Wu, S. Lee, J. Gao, Photocatalytic performance of plasma sprayed Pt-modified $TiO_2$ coatings under visible light irradiation, Catal. Commun. 8 (2007) 906–912.
[43] D. Behar, J. Rabani, Kinetic of hydrogen prodcution upon reduction of aqueous $TiO_2$ nanoparticles catalyzed by $Pd^0$, $Pt^0$, or $Au^0$ coatings and an unusual hydrogen abstraction; steady state and pulse radiolysis study, J. Phys. Chem. B 110 (2006) 8750–8755.
[44] C. Clavero, Plasmon-induced hot-electron generation at nanoparticle/metal-oxide interfaces for photovoltaic and photocatalytic devices, Nat. Photonics 8 (2014) 95–103.
[45] K. Qian, B.C. Sweeny, A.C. Johnston-Peck, W. Niu, J.O. Graham, J.S. DuChene, J. Qiu, Y.C. Wang, M.H. Engelhard, D. Su, E.A. Stach, W.D. Wei, Surface plasmon-driven water reduction: gold nanoparticle size matters, J. Am. Chem. Soc. 136 (2014) 9842–9845.
[46] Y. Tian, T. Tatsuma, Plasmon-induced photoelectrochemistry at metal nanoparticles supported on $TiO_2$, Chem. Commun. 1810–1811 (2004).
[47] M. Matsuoka, M. Anpo, Applications of environmentally friendly $TiO_2$ photocatalysts in green chemistry: environmental purification and clean energy poduction under solar light irradiation, in: P.T. Anastas, R.H. Crabtree (Eds.), Handbook of Green Chemistry, Wiley-VCH Verlag GmbH & Co. KGaA, Weinheim, 2010, pp. 59–80.
[48] S.C. Gad, K.L. Sharp, C. Montgomery, J.D. Payne, G.P. Goodrich, Evaluation of the toxicity of intravenous delivery of auroshell particles (gold-silica nanoshells), Int. J. Toxicol. 31 (2012) 584–594.
[49] O. Khantamat, C.H. Li, F. Yu, A.C. Jamison, W.C. Shih, C. Cai, T.R. Lee, Gold nanoshell-decorated silicone surfaces for the near-infrared (NIR) photothermal destruction of the pathogenic bacterium *E. faecalis*, ASC Appl. Mater, Interfaces 7 (2015) 3981–3993.
[50] T. Pham, J.B. Jackson, N.J. Halas, T.R. Lee, Preparation and characterization of gold nanoshells coated with self-assembled monolayers, Langmuir 18 (2002) 4915–4920.
[51] C. Sun, Y. Wu, W. Zhang, N. Jiang, T. Jiu, J. Fang, Improving efficiency by hybrid $TiO_2$ nanorods with 1,10-phenanthroline as a cathode buffer layer for inverted organic solar cells, ASC Appl. Mater. Interfaces 6 (2014) 739–744.
[52] K. Tanaka, M.F.V. Capule, T. Hisanaga, Effect of crystallinity of $TiO_2$ on its photocatalytic action, Chem. Phys. Lett. 187 (1991) 73–76.
[53] T. Ohno, K. Sarukawa, M. Matsumura, Photocatalytic activities of pure rutile particles isolated from $TiO_2$ powder by dissolving the anatase component in HF solution, J. Phys. Chem. B 105 (2001) 2417–2420.
[54] J. Jiang, G. Oberdörster, A. Elder, R. Gelein, P. Mercer, P. Biswas, Does nanoparticle activity depend upon size and crystal phase?, Nanotoxicology 2 (2008) 33–42
[55] B.L. Bischoff, M.A. Anderson, Peptization process in the sol-gel preparation of porous anatase ($TiO_2$), Chem. Mater. 7 (1995) 1772–1778.
[56] X.Z. Ding, Z.Z. Qi, Y.Z. He, Effect of hydrolysis water on the preparation of nano-crystalline titania powders via a sol-gel process, J. Mater. Sci. Lett. 14 (1995) 21–22.
[57] D. Vorkapic, T. Matsoukas, Effect of temperature and alcohols in the preparation of titania nanoparticles from alkoxides, J. Am. Ceram. Soc. 81 (1998) 2815–2820.
[58] T. Zeng, Y. Qiu, L. Chen, X. Song, Microstructure and phase evolution of $TiO_2$ precursors prepared by peptization-hydrolysis method using polycarboxylic acid as peptizing agent, Mater. Chem. Phys. 56 (1998) 163–170.
[59] S. Auvinen, M. Alatalo, H. Haario, J.P. Jalava, R.J. Lamminmaki, Size and shape dependence of the electronic and spectral properties in $TiO_2$ nanoparticles, J. Phys. Chem. C 115 (2011) 8484–8493.
[60] R.W. Cheyne, T.A.D. Smith, L. Trembleau, A.C. Mclaughlin, Synthesis and characterisation of biologically compatible $TiO_2$ nanoparticles, Nanoscale Res. Lett. 6 (2011) 1–6.
[61] S. Horikoshi, N. Serpone, Introduction to nanoparticles, in: S. Horikoshi, N. Serpone (Eds.), Microwaves in Nanoparticle Synthesis: Fundamentals and Applications, Wiley-VCH Verlag GmbH & Co. KGaA, Weinheim, 2013, pp. 1–24.
[62] L. Du, A. Furube, K. Yamamoto, K. Hara, R. Katoh, M. Tachiya, Plasmon-induced charge separation and recombination dynamics in gold-$TiO_2$ nanoparticle systems: dependence on $TiO_2$ particle size, J. Phys. Chem. C 113 (2009) 6454–6462.
[63] D. Zhou, Z. Ji, X. Jiang, D.R. Dunphy, J. Brinker, A.A. Keller, Influence of material properties on $TiO_2$ nanoparticle agglomeration, PLoS ONE 8 (2013) 1–7.
[64] M. Horn, C.F. Schwerdtfeger, E.P. Meagher, Refinement of structure of anatase at several temperatures, Z. Kristallogr. 136 (1972) 273–281.
[65] J.I. Langford, A.J.C. Wilson, Scherrer after sixty years: a survey and some new results in the determination of crystallite size, J. Appl. Crystallogr. 11 (1978) 102–113.
[66] J. Zhang, X. Jin, P.I. Morales-Guzman, X. Yu, H. Liu, H. Zhang, L. Razzari, J.P. Claverie, Engineering the absorption and field enhancement properties of Au-$TiO_2$ nanohybrids via whispering gallery mode resonances for photocatalytic water splitting, ACS Nano 10 (2016) 4496–4503.
[67] Z.W. Seh, S. Liu, M. Low, S.Y. Zhang, Z. Liu, A. Mlayah, M.Y. Han, Janus Au-$TiO_2$ photocatalysts with strong localization of plasmonic near-fields for efficient visible-light hydrogen generation, Adv. Mater. 24 (2012) 2310–2314.
[68] S.T. Kochuveedu, D.P. Kim, D.H. Kim, Surface-plasmon-induced visible light photocatalytic activity of $TiO_2$ nanospheres decorated by Au nanoparticles with controlled configuration, J. Phys. Chem. C 116 (2012) 2500–2506.
[69] B. Erdem, R.A. Hunsicker, G.W. Simmons, E.D. Sudol, V.L. Dimonie, M.S. El-Aasser, XPS and FTIR surface characterization of $TiO_2$ particles used in polymer encapsulation, Langmuir 17 (2001) 2664–2669.
[70] M.Z. Iqbal, M.S. Katsiotis, S.M. Alhassan, M.W. Liberatore, A.A. Abdala, Effect of solvent on the uncatalyzed synthesis of aminosilane-functionalized graphene, RSC Adv. 4 (2014) 6830–6839.
[71] R.J. Hunter, Zeta Potential in Colloid Science: Principles and Applications, first ed., Academic Press, San Diego, 1981.
[72] B. Salopek, D. Krasić, S. Filipović, Measurement and application of zeta-potential, RGN Zbornik 4 (1992) 147–151.
[73] S.E. Park, M.Y. Park, P.K. Han, S.W. Lee, The effect of pH-adjusted gold colloids on the formation of gold clusters over APTMS-coated silica cores, Bull. Korean Chem. Soc. 27 (2006) 1341–1345.
[74] E. Cano, C.L. Torres, J.M. Bastidas, An XPS study of copper corrosion originated by formic acid vapour at 40% and 80% relative humidity, Mater. Corros. 52 (2001) 667–676.
[75] S. Naya, A. Inoue, H. Tada, Visible-light activity enhancement of gold-nanoparticle-loaded titanium(IV) dioxide by preferential excitation of localized surface plasmon resonance, ChemPhysChem 12 (2011) 2719–2723.
[76] S.J. Oldenburg, S.L. Westcott, R.D. Averitt, N.J. Halas, Surface enhanced Raman scattering in the near infrared using metal nanoshell substrates, J. Chem. Phys. 111 (1999) 4729–4735.
[77] V. Amendola, R. Pilot, M. Frasconi, O.M. Maragò, M.A. Iatì, Surface plasmon resonance in gold nanoparticles: a review, J. Phys.: Condens. Matter 29 (2017) 203002.
[78] H. Yamashita, Y. Ichihashi, S.G. Zhang, Y. Matsumura, Y. Souma, T. Tatsumi, M. Anpo, Photocatalytic decomposition of NO at 275 K on titanium oxide catalysts anchored within zeolite cavities and framework, Appl. Surf. Sci. 121 (1997) 305–309.
[79] J. Shi, J. Chen, Z. Feng, T. Chen, Y. Lian, X. Wang, C. Li, Photoluminescence characteristics of $TiO_2$ and their relationship to the photoassisted reaction of water/methanol mixture, J. Phys. Chem. C 111 (2007) 693–699.
[80] H. Tang, K. Prasad, R. Sanjinès, P.E. Schmid, F. Lévy, Electrical and optical-properties of $TiO_2$ anatase thin-films, J. Appl. Phys. 75 (1994) 2042–2047.
[81] H. Tang, H. Berger, P.E. Schmid, F. Lévy, G. Burri, Photoluminescence in $TiO_2$ anatase single-crystals, Solid State Commun. 87 (1993) 847–850.
[82] S.M. Kim, S.J. Lee, S.H. Kim, S. Kwon, K.J. Yee, H. Song, G.A. Somorjai, J.Y. Park, Hot carrier-driven catalytic reactions on Pt-CdSe-Pt nanodumbbells and Pt/GaN under light irradiation, Nano Lett. 13 (2013) 1352–1358.